



1 **Holocene hydrography evolution in the Alboran Sea: a multi-record and**
2 **multiproxy comparison**

3

4 **Albert Català¹, Isabel Cacho¹, Jaime Frigola¹, Leopoldo D. Pena¹ and Fabrizio**
5 **Lirer²**

6

7 ¹ Grup de Recerca Consolidat en Geociències Marines, Departament de Dinàmica de
8 la Terra i de l'Oceà, Universitat de Barcelona (UB), Barcelona, Spain.

9 ² Istituto di Science Marine (ISMAR) -CNR, sede di Napoli, Italy

10

11

12

13 **Corresponding author:**

14 Albert Català, GRC Geociències Marines, Dept. Dinàmica de la Terra i de l'Oceà,
15 Facultat de Geologia. C/ Martí i Franquès s/n 08028, Barcelona. Universitat de
16 Barcelona

17 Email address: al_catala@ub.edu

18



19 **ABSTRACT**

20 A new high resolution deglacial and Holocene Sea Surface Temperature (SST)
21 reconstruction is presented for the Alboran Sea (western Mediterranean), based on
22 Mg/Ca ratios measured in the planktonic foraminifera *Globigerina bulloides*. This new
23 record is evaluated by comparison with other Mg/Ca – SST and previously published
24 alkenone-SST reconstructions from the same region for both Holocene and glacial
25 period. In all cases there is a high degree of coherence between the different Mg/Ca-
26 SST records but strong discrepancies when compared to the alkenone-SST records. We
27 argue that these discrepancies are due to differences in the proxy-response during
28 deglaciation which we hypothesize to reflect a resilience strategy of *G. bulloides*
29 changing its main growth season. In contrast, short-term Holocene SST variability is
30 larger in the Mg/Ca-SST than in the alkenone-SST records. It is proposed that larger
31 Mg/Ca-SST variability to be the result of spring season variability, while the smoothed
32 alkenone-SST variability represents average annual temperatures. Mg/Ca-SST record
33 differentiates the Holocene in three periods (1) The warmest SST values occurred during
34 the Early Holocene (11.7 – 9 kyr BP); (2) During the middle Holocene occurred a
35 continuous cooling trend that culminated with the coldest Holocene SST in a double peak
36 structure centred at around 4.2 kyr BP; (3) The Late Holocene (4.2 kyr BP to the present)
37 did not follow any clear cooling/warming trend but millennial-scale oscillations were
38 enhanced. This SST evolution is discussed in the context of changing properties in the
39 Atlantic inflow associated to North Atlantic circulation conditions and also to local
40 hydrographical and atmospheric changes. To conclude, we propose a tight link between
41 North Atlantic circulation patterns and inflow of surface waters into the Mediterranean
42 playing a major role in the controls of Holocene climatic variability of this region.

43

44 **1. INTRODUCTION**



45 The Holocene climate evolution in general, and also in the Alboran Sea (11.7 kyr BP to
46 present) is considered more stable than the last glacial period (Bond et al., 1997; Cacho
47 et al., 1999; Martrat et al., 2014). However, there is an increasing number of Holocene
48 climate records revealing significant changes in both long term patterns, orbital forcing
49 (e.g. Marchal et al., 2002; Lorenz and Lohmann 2004; Tzedakis, 2007; Wanner et al.,
50 2008; Tinner et al., 2009; Bartlein et al., 2011), and also to millennial and centennial-
51 scale variability (e.g. Bond et al., 1997, 2001; Andrews et al., 2003; Marchitto and
52 deMenocal, 2003; Moros et al., 2004; Debret et al. 2007 and 2009; Thornalley 2009;
53 Giraudeau et al., 2010). In the ocean context and concretely over the North Atlantic
54 Ocean, there are solid evidences about Holocene changes in several oceanographic
55 parameters linked to Atlantic Meridional Overturning Circulation (AMOC) like the heat
56 exchange within the subpolar gyre (SPG) and the subtropical gyre (STG) (Bond et al.,
57 1997, 2001; Thornalley et al., 2009; Colin et al., 2010; Repschläger et al., 2017). Studies
58 on Holocene atmospheric conditions over the North Atlantic region suggest the
59 occurrence of northward and southward displacements of the winter storm tracks
60 (Fletcher et al., 2012; Desprat et al., 2013; Chabaud et al., 2014; Zielhofer et al., 2017).
61 The Western Mediterranean Sea is very sensitive to changes in the Atlantic Ocean
62 conditions. These oceanic and atmospheric connections have been well documented
63 and described for the last glacial period (Cacho et al., 1999; Moreno et al., 2002; Sierro
64 et al., 2005; Frigola et al., 2008; Toucane et al., 2012) when intense millennial-scale
65 variability occurred associated to major changes in the AMOC (the so-called Dansgaard-
66 Oeschger cycles and Heinrich events). However, even though the Holocene climate
67 variability over the western Mediterranean has also been extensively studied (i.e: Cacho
68 et al., 2001; Frigola et al., 2007, Rodrigo-Gàmiz 2011; Ausin et al, 2015; Jalali et al.,
69 2016), unlike the glacial periods, any potential connection with the changes occurred in
70 the North Atlantic Ocean remains unclear.



71 One of the limitations in the study of Holocene climate variability relies on the sensitivity
72 of our proxies. During this period, the natural range of variability for SST or $\delta^{18}\text{O}_{\text{SW}}$ are
73 relatively short and, these natural changes are often below the magnitude of the proxy
74 sensitivity. For this reason, to validate the climate value of proxy signals for the Holocene,
75 it becomes critical to reproduce them in comparable records and ideally, with
76 independent proxies. With this aim, here we present a new high resolution Holocene
77 SST record based on the Mg/Ca ratio in the planktonic foraminifera *G. bulloides* in core
78 ALB-2 from the Alboran Sea. The information of this record is also compared with other
79 three Mg/Ca-SST records, two new (MD95-2043 and MD99-2343) and other previously
80 published (ODP 976; Jimenez-Amat and Zahn 2015) and all of them are from the
81 Western Mediterranean Sea and based on *G. bulloides*. The Western Mediterranean
82 Sea has been intensively studied previously and several SST records exist mostly based
83 in the application of the $U^{K_{37}}$ index measured on alkenones (Cacho et al., 2001; Martrat
84 et al., 2004; Rodrigo-Gámiz 2014; Ausin et al., 2015). This multi-core and multi-proxy
85 approach comparison lets into the discussion of the proxy limitations to identify some
86 SST changes with discrepancies between the two considered proxies. The new high-
87 resolution Mg/Ca-SST let us to discuss the Holocene-SST evolution in this region and
88 hypothesize some potential connection with changes in the North Atlantic Ocean.

89

90 **2. REGIONAL SETTINGS**

91 Climate in the western Mediterranean region is characterized by warm and dry summers
92 while autumn and winter are mild and humid. During winters, westerly winds are
93 predominant displacing the storm tracks to southern positions and thus supplying humid
94 conditions over the western Mediterranean region. (Trigo et al., 2002; Combourieu
95 Nebout et al., 2009; Fletcher et al., 2012; Roberts et al., 2012; Nieto-Moreno et al., 2013).
96 At the end of summer and the early autumn the temperature differences between the air



97 masses and the surface Mediterranean can produce violent precipitation events (Lionello
98 et al., 2006 Sabatier et al., 2012).

99 The Alboran Sea oceanography is controlled by the water masses exchange between
100 the Mediterranean and the Atlantic Ocean. The low-salinity Atlantic waters enter to the
101 Mediterranean Sea as a surface layer while high salinity waters from the Mediterranean
102 outflow into the Atlantic Ocean as a deeper-water mass (Mediterranean Outflow Water,
103 MOW). Surface waters at the Alboran Sea are typically defined as Modified Atlantic
104 Water (MAW), composed mainly by a mixing of Surface Atlantic Water (SAW) and the
105 Eastern North Atlantic Central Water (ENACW) (Bray et al., 1995; Millot, 2009) (Fig.1a
106 and b). This ENACW has been characterized by central waters from two different
107 sources areas converging in the northwest of the Iberian Peninsula. One source has a
108 subpolar origin (ENACWsp) which is formed near 46°N around the Celtic Sea
109 (McCarteney and Talley, 1982). The other source has a subtropical origin (ENACWst)
110 formed near 35°N around the Azores Islands (Fiúza, 1984) (Fig. 1a). Hydrographic
111 properties of these water masses are related to changes in heat and salt transport
112 through the STG – SPG that ultimately modulate the AMOC (ie: Cléroux et al., 2012;
113 Thornalley., 2009; Gao and Yu 2008; Böning et al., 2006). MAW describes two
114 anticyclonic gyres at the Alboran Sea (Western and Eastern Alboran Gyres, WAG and
115 EAG) when it progresses eastwards changing its proprieties (Fig 1b). The ALB-2 core is
116 located in the center of the WAG. Sediment fluxes based in sediments traps from the
117 same location showed relatively high values attributed to a funneling effect by the gyre
118 capturing particles from the edges toward the center (Fabres et al., 2002).

119

120 **3. MATERIALS AND METHODS**

121 Core HER-GC-ALB2 (here abbreviated as ALB-2) was retrieved from the Alboran Sea
122 (Lat: 36°0'44.80"N; Log: 4°16'24.38"W; 1313 mwd) during the HERMESIONE cruise in



123 2009 (Fig.1b), on board of BIO Hespérides. Core ALB-2 was drilled with a gravity core
124 system and covers a continuous sequence of 337 cm length.

125 Geochemical analysis were performed on the planktonic foraminifera *Globigerina*
126 *bulloides*. The individual specimens were hand-picked between 250 – 355 μm size
127 fractions in order to obtain a homogenous population. The selected specimens presented
128 apparently well-preserved and clean shells.

129 3.1 Stable Isotopes

130 Around 10 specimens of *G. bulloides* per sample were crushed between two glasses
131 under the binocular microscope in order to open the chambers and allow the cleaning of
132 the shells interior. Samples were cleaned with 500 μl of methanol in an ultrasonicated
133 bath during 30 seconds in order to mobilize the clay residues. The residual methanol
134 was removed and samples dried prior to analysis. The analyses were performed with an
135 isotope-ratio mass spectrometry (IRMS) Finnigan-MAT 252 linked online to a single acid
136 bath CarbonKiel-II carbonate preparation device at Scientific and Technological Centre
137 (CCiT) of the University of Barcelona. The analytical precision of laboratory standards
138 for $\delta^{18}\text{O}$ was better than 0.08 ‰. Calibration to Vienna Pee Dee Belemnite (VPDB) was
139 carried out by means of NBS-19 standards (Coplen, 1996).

140 Seawater $\delta^{18}\text{O}$ ($\delta^{18}\text{O}_{\text{sw}}$) was obtained after removing the temperature effect, with the
141 Shackleton paleotemperature equation (Shackleton, 1974) on the *G. bulloides* $\delta^{18}\text{O}$
142 signal using the *G. bulloides* Mg/Ca–SST values. The results are expressed in the
143 SMOW (Standard Mean Ocean Water) water standard ($\delta^{18}\text{O}_{\text{sw}}$) after the correction of
144 Craig (1965).

145 3.2 Chronologies

146 Chronology from core ALB-2 is based on fourteen ^{14}C AMS dates measured in planktonic
147 foraminifera samples handpicked from the 215 – 355 μm fraction (8 – 33 mg). The top



148 ten radiocarbon dates are based on monospecific samples of *Globigerina inflata*, and
149 the four older dates are based on multispecific samples of planktonic foraminifera
150 (Supplement Table S1). Radiocarbon ages were calibrated with the MARINE13
151 calibration curves (Reimer, et al., 2013). The age model was build using the Bayesian
152 statistics software Bacon with the statistical package R (Blaaw and Christien, 2011) for
153 marine sediments (Supplementary Figure S2). From the core top to the first ^{14}C AMS
154 date (10 cm), the age model was performed by a linear regression assuming the age of
155 the core top to be that of the sediment core recovery (2009 yr CE or -59 yr BP). The
156 chronology at the base of the core was established by isotopic stratigraphy by correlating
157 a well-expressed positive excursion in the $\delta^{18}\text{O}$ -ALB2 to a well dated comparable
158 structure in the $\delta^{18}\text{O}$ -MD95-2043 measured in both cases on *G. bulloides*
159 (Supplementary Table S1 and Supplementary Figure S2). According to the generated
160 age model, core ALB-2 covers the last 15 kyr BP with an average sedimentation rate of
161 22 cm/kyr that provides a time resolution of about 45 yr for the applied sampling interval
162 (1 cm).

163 Age model for MD99-2343 was improved from that originally published by Frigola et al.
164 (2007) in base to nine new ^{14}C AMS dates incorporated to the previous age model
165 (Supplement Table S3). The updated age model is provided with nineteen ^{14}C AMS
166 recovering the last 17 kyr BP. This age model update was built using the Bayesian
167 statistics software Bacon with the statistical package R (Blaaw and Christien, 2011) for
168 marine sediments (Supplementary Figure S4). The age of the core top was assumed to
169 be the recovered year (1999 yr CE or -49 yr BP). The chronology during the deglaciation
170 was improved by adding two tie points by correlating a marked $\delta^{18}\text{O}$ structure in both the
171 Menorca core MD99-2343 and the Alboran core MD95-2043 (Supplementary Table S3
172 and Supplementary S4).

173 **3.3 *G. bulloides* Mg/Ca ratios and Sea Surface Temperatures estimates**



174 Mg/Ca measurements in core ALB-2 were done over samples containing 50-60
175 specimens of *G. bulloides*, gently crushed between two glasses under the binocular in
176 order to open the chambers and allow the removal of contaminant phases from the shell
177 interior. The cleaning protocol for the foraminifera shells was based on the full procedure
178 described by Pena et al. (2005) which includes the reductive step. Once cleaned each
179 sample was dissolved in ultra-pure acid nitric 1% with Rh as an internal standard. After
180 dissolution, samples were centrifuged to remove any potential un-dissolved mineral
181 particles. Procedural blanks were routinely produced to detect any potential
182 contamination problem during the sample cleaning and dissolution process.

183 Instrumental analysis were performed in an ICP-MS Perkin-Elmer Elan-6000 at the
184 CCI-T-UB. Every four samples, a standard solution was analysed. The standard solution
185 was prepared gravimetrically with known concentrations of Mg, Ca, Mn, and Al, and
186 produced with a ratio (element/Ca) comparable to that expected for the samples.
187 Analytical reproducibility obtained in base to the gravimetric standard samples was
188 98.38% for the Mg/Ca ratio. Moreover, all Mg/Ca ratios in this core were corrected using
189 the same gravimetric standard for each ICP-MS round using a sample-standard
190 bracketing (SSB) method providing a valid solution with high-precision and accuracy of
191 every sample measurement.

192 The obtained *G. bulloides* Mg/Ca ratios were then compared with other analysed ratios,
193 i.e. Al/Ca and Mn/Ca, in order to identify potential contaminations of remaining
194 manganese oxides and/or aluminosilicates in the samples (Barker et al., 2003; Pena et
195 al., 2005). Such potential contamination could provide anomalous high *G. bulloides*
196 Mg/Ca ratios and therefore, overestimating the inferring SST values. In the ALB-2 record,
197 Mn/Ca ratios above 2σ (0.29 mmol/mol) were removed (Supplementary Figure S5a). The
198 Al/Ca ratio was considered to potentially indicate presence of un-removed silicates (likely
199 clays) and those samples with values above 2σ (1.74 mmol/mol) were also removed
200 (Supplementary Figure S5b).



201 *G. bulloides* Mg/Ca records from cores MD95-2043 and MD99-2343 were produced
202 following a comparable procedure to that described for the ALB-2 core but, for these
203 cores, the data to estimate analytical reproducibility and the Mn/Ca and Al/Ca ratios to
204 evaluate the potential interference of contamination phases were not available.
205 Consequently, the uncertainties associated with these complementary SST-records are
206 larger than those associated with the ALB-2 sediment core, which is the main focus of
207 this study. *G. bulloides* Mg/Ca ratios from core ODP 976, also included in the discussion,
208 were already published by Jiménez-Amat and Zahn (2015).

209 The *G. bulloides* Mg/Ca ratios of the four discussed sediment cores have been
210 transferred to SST applying the calibration from Cisneros et al. (2016). This calibration
211 is based on those *G. bulloides* Mg/Ca ratios available from core top samples of the North
212 Atlantic Ocean (Elderfield and Gansen, 2000) and the addition of core top samples from
213 the western Mediterranean Sea. These Mediterranean samples enhance the
214 temperature range of the original calibration toward the warmer edge and thus, the
215 obtained calibration covers better the oceanographic conditions of the western
216 Mediterranean Sea. This calibration provides realistic SST for the *G. bulloides* bloom
217 season around April-May over the western Mediterranean Sea (Cisneros et al., 2016).

218

219 **4. RESULTS AND DISCUSSION**

220 **4.1 Holocene evolution in western Mediterranean *G. bulloides* – $\delta^{18}\text{O}$ records**

221 The new $\delta^{18}\text{O}$ record from ALB-2 is compared with other previously published high
222 resolution $\delta^{18}\text{O}$ -records from the western Mediterranean Sea (Cacho et al., 1999; Frigola
223 et al., 2007; Jiménez-Amat and Zahn 2015) in order to evaluate the regional significance
224 of the recorded signal (Fig. 2). The main patterns in the $\delta^{18}\text{O}$ records show an
225 extraordinary resemblance between them and even several centennial scale structures
226 can be correlated through the cores, taking into account the individual core chronological



227 uncertainties. The isotopic depletion associated with the last termination ends in all four
228 records at around 9 kyr BP. Along the Holocene all the *G. bulloides* $\delta^{18}\text{O}$ records are
229 rather stable, with several short oscillations (0.2-0.3‰) and a slight enrichment trend
230 toward the late Holocene (Fig. 2). This comparison supports the regional value of the
231 captured paleoceanographical signal and the robustness of the individual age models.

232 In terms of absolute values of *G. bulloides* $\delta^{18}\text{O}$ records, clear differences can be
233 detected between the different cores. Both ALB-2 and ODP976 cores, located in the
234 westernmost part of the Alboran Sea, display the lightest values (note that curves in Fig.
235 2b are plotted with independent y axis). While core MD95-2043 located in the eastern
236 part of the Alboran Sea show heavier $\delta^{18}\text{O}$ values than the other two Alboran records
237 (Fig. 2b). Finally, core MD99-2343, located north of Minorca Island, shows the heaviest
238 $\delta^{18}\text{O}$ values. Such isotopic pattern is consistent with the regional oceanography, showing
239 the lightest $\delta^{18}\text{O}$ values in those sites with stronger influence of North Atlantic surface
240 inflow while $\delta^{18}\text{O}$ values become heavier along its path into the Mediterranean Sea. This
241 situation reflects the excess of evaporation of the Mediterranean Sea (Béthoux, 1980;
242 Lacombe et al., 1981) that results in an enhancement of the salinity but also of the marine
243 water $\delta^{18}\text{O}$ values. It is interesting to note that the presented isotopic records show a
244 strong gradient between the western and eastern Alboran Sea (of about 0.5‰), probably
245 due to a strong surface mixing with the underlying Mediterranean waters originated by
246 the two anticyclonic gyres (Tintore et al., 1988; Millot., 1999), and supporting that the
247 Atlantic Inflow became rapidly modified along the Alboran Sea. The isotopic change from
248 the eastern Alboran Sea core (MD95-2043) and the Menorca core (MD99-2343) is even
249 larger (of about 0.7‰) reflecting the long path of these inflowing Atlantic waters through
250 the western Mediterranean Sea until reaching the Menorca location.

251 **4.2 Sea Surface Temperatures: Multi-record and multi-proxy comparison**

252 According to the ALB-2 Mg/Ca-SST record, the Holocene maximum temperatures
253 ($18.3\pm 1.4^\circ\text{C}$; uncertainties of average values represent 1σ ; uncertainties of absolute



254 values are those derived from the Mg/ Ca–SST calibration) were reached at the onset of
255 the Holocene ~11.0 kyr (Fig. 3b) and a general cooling trend until the present
256 characterizes the record, punctuated by several short term oscillations (maximum of
257 2°C). However, the ALB-2 SST record can be divided in three main intervals. The first
258 interval correspond to most of the Early Holocene (11.7 – 9 kyr BP) when SST were
259 warmest and relatively stable (no significant trend) oscillating at around an average value
260 of $\sim 16.2 \pm 1.3^\circ\text{C}$ (Fig. 3b). The second interval displays a general cooling trend of $\sim 4^\circ\text{C}$
261 ending at around 4.2 kyr BP when minimum Holocene SSTs were reached
262 ($\sim 12.8 \pm 1.1^\circ\text{C}$) (Fig. 3b). The last and most recent interval does not show any clear
263 warming/cooling trend although shows warmer SST than previous interval (average SST
264 of $\sim 14 \pm 1.2^\circ\text{C}$) and intense SST oscillations ($\sim 1.2^\circ\text{C}$) of longer duration than those
265 recorded during previous intervals (Fig. 3b).

266 The ALB-2 *G. bulloides* Mg/Ca-SST record has been compared to other three SST
267 records from the western Mediterranean Sea that were calculated following the same
268 Mg/Ca-SST procedure (Fig. 3b-e). The chronologies of the four compared records are
269 very robust (Fig. 2c) and totally independent for the Holocene period (ALB-2 and MD99-
270 2343: This study; ODP976: Combourieu Nebout et al., 2002; MD95-2043: Cacho et al.,
271 1999). The sampling resolution of the ALB-2 record is higher than in the other sites, but
272 the main patterns agree well between all the compared records. Maximum SST occurred
273 around 11 kyr BP in all records, and also a general cooling trend can be observed during
274 Early-Mid Holocene ending in all cases before the Late Holocene (Fig. 3b-e). Absolute
275 values also show a good agreement, when the resolution is high enough, some millennial
276 scale structures can even be correlated between the four records. This multi-core
277 comparison strongly supports the value of *G. bulloides* Mg/Ca in this region as a SST
278 proxy, and gives confidence that the obtained SST records reflect true regional
279 environmental conditions. Nevertheless, these Mg/Ca-SST reconstructions show evident
280 differences with the previous published SST reconstructions based on alkenones



281 measurements that needs a further discussion (Fig.3f; Cacho et al., 2001; Martrat et al.,
282 2004 and 2014; Jiménez-Amat and Zahn 2015).

283 Alkenones-SST reconstructions are based on the relative abundance of di and tri-
284 unsaturated C₃₇ alkenones mostly produced in the Alboran Sea by the marine
285 coccolithophore *Emiliania huxleyi* (Valkman et al., 1980; Prah1 et al., 2000; Ausin et al.,
286 2015). The comparison between *G. bulloides* Mg/Ca-SST and alkenones-SST (also
287 studied by Jiménez-Amat and Zahn 2015) shows remarkable differences in both
288 absolute values and main patterns, even when both proxies are measured on the same
289 core, as it can be observed in core MD95-2043 and also ODP 976 (Fig. 3d and f). For
290 the Holocene period, maximum SST in the alkenones record was reached latter (~10 kyr
291 BP) than in Mg/Ca-SST records, and thenceforth the alkenones-SST record shows a
292 rather flat pattern for the whole Holocene, with a slight cooling trend of about 1°C. In
293 contrast, ALB-2 *G. bulloides* Mg/Ca-SST (Fig. 3b) show larger variability in the long term
294 but also in the short term variability. Holocene absolute SST values in the alkenones
295 record are warmer (20-18°C) than those recorded by the Mg/Ca record (18-13°C).

296 Alkenones-SST records have been interpreted to reflect an annual average (Prah1, et al.,
297 2000; Cacho et al., 2001, Martrat et al., 2004, 2014) although slightly biased toward the
298 colder values since coccolith productivity during the very stratified and oligotrophic
299 summer months of the Mediterranean Sea is limited (Ternois et al., 1996; Sicre et al.,
300 1999; Bárcena et al., 2004; Versteegh et al., 2007; Hernández-Almeida et al., 2011). In
301 contrast, the Mg/Ca-SST record in the western Mediterranean Sea has been argued to
302 show a narrower seasonal window, in particular during spring months (April-May)
303 (Bárcena et al., 2004; Cisneros et al., 2016). This observation agrees with the
304 preferential habitat of *G. bulloides* that needs nutrient supply by vertical mixing (Rao et
305 al., 1988; Hemleben et al., 1989; Kemle-von Mücke and Hemleben, 1999; Bárcena et
306 al., 2004). Moreover maxima foraminifera fluxes in sediment traps from the western
307 Mediterranean Sea are concentrated in April-May, even that in autumn months



308 (November-December) a second small increase can also occur (Bárcena et al., 2004;
309 Rigual-Hernández, 2012). Current SSTs in the Alboran Sea are on average 17.9 °C, 18.3
310 °C and 18.7°C, for spring months, autumn and on annual average, respectively (Shaltout
311 and Omstedt., 2014). Consequently, alkenones-Mg/Ca SST offset may reflect both
312 seasonal but also depth differences between *E. huxleyi* and *G. bulloides* habitats. The
313 rather smooth behaviour of the alkenone signal, in contrast to the Mg/Ca signal, has
314 previously been recognised and attributed to the intrinsic characteristics of the proxy
315 measurements (Laepplé and Huybers, 2013). The number of individuals that integrates
316 the SST signal in a single measurement is of several orders the magnitude larger in the
317 alkenones than in the Mg/Ca analyses (Laepplé and Huybers, 2013). This situation
318 favours the integration of several seasons and years in the alkenone-SST signal while
319 Mg/Ca-SST signal will be more sensitive to seasonal and inter-annual variability
320 (Jiménez-Amat and Zahn 2015) In base to these observations, we interpret that the
321 Mg/Ca-SST appears to represent better spring season variability, allowing to
322 characterise better the short and long term SST variability during the relatively stable
323 Holocene period.

324 But the most remarkable difference between the Mg/Ca and alkenones SST
325 reconstructions corresponds to the deglacial period (at the end of GS-1 or Younger Dryas
326 - YD). Both alkenones and Mg/Ca SST records show a cooling of about ~3 – 4°C at the
327 onset of the GS-1 (YD) but the big difference occurs at the end of this interval. Both
328 alkenones and Mg/Ca records show an intra-YD first warming (Cacho et al., 2001) and
329 then alkenones SST continues the deglacial warming while Mg/Ca record shows a
330 cooling. In order to explore better this proxy discrepancies we have also compared these
331 two records for the glacial period in Figure 4. *G. bulloides* Mg/Ca-SST during the last
332 glacial period record the same oscillations and absolute values than alkenones-SST,
333 they both agree in the first warming of the deglaciation but clearly, the second warming
334 phase of the deglaciation does not appears in the Mg/Ca record (Fig. 4). The absence



335 of SST warming during the second phase of the deglaciation can be observed in the four
336 Mg/Ca records presented in Figure. 3. Thus, this is a proxy characteristic that may reflect
337 the limited capacity of *G. bulloides* to adapt to the large temperature change occurring
338 during the deglaciation. *G. bulloides* has different genotypes adapted to different ranges
339 of water temperatures, from transitional to subpolar water (Kucera and Darling 2002;
340 Kucera et al., 2005) but they start to be scarce in water with temperatures over 18°C.
341 This agrees with the maximum temperatures recorded during both glacial and interglacial
342 periods in the Mg/Ca records (Fig. 4). Consequently we interpret that *G. bulloides* has a
343 resilient capacity to change the growth season in order to survive the large deglacial-
344 SST changes in the region. We propose that during the glacial period and the first part
345 of deglaciation *G. bulloides* could have had its maximum representation during the
346 autumn bloom when upwelling conditions reappear after the warm sea summer
347 stratification. That could have allowed *G. bulloides* to grow in a relatively mild upwelling
348 season during the glacial period. Nowadays autumn SST values are comparable to the
349 annual average SST values and that could explain the comparable SST values of both
350 alkenones and Mg/Ca proxies. However the second deglacial warming could have been
351 too extreme for *G. bulloides* and they would have moved to the spring upwelling bloom
352 with colder SSTs than those during autumn. Consequently we hypothesize that the
353 absence of the second deglacial warming in the *G. bulloides*-Mg/Ca record may reflect
354 a resilience strategy to change its habitat. Upon entering the Holocene, when SST
355 variability was shorter and within its habitat tolerance, *G. bulloides* became a good
356 sensor of interglacial SST variability (Fig. 3 and 4).

357 **4.3 Holocene evolution in Alboran surface hydrography**

358 The overall Holocene SST evolution in the Alboran Sea is described in three different
359 phases (Fig. 5c): (a) maximum SST during the early Holocene (11 - 9 kyr BP); (b) cooling
360 trend across the middle Holocene (9 – 4.2 kyr BP); (c) relatively colder temperatures with
361 intense millennial-scale oscillations for the late Holocene (4.2 – 0 kyr BP). This general



362 SST pattern also agrees well with that described for the North Atlantic and Western
363 Mediterranean Sea in base to regional data compilation (Marchal et al., 2002; Kim et al.,
364 2004; Rimbu et al., 2004; Wanner et al., 2008) and with the expected Holocene
365 redistribution of solar energy by the changing orbital configuration according to
366 atmosphere-ocean general circulation model (Fig. 5a and c; Lorenz and Lohmann 2004).
367 Nevertheless, the intensity of the Holocene SST changes in the Alboran Sea (over 5°C)
368 exceeds that expected by simply orbital changes in insolation (~1.6°C in atmosphere)
369 (Lorenz and Lohmann 2004), therefore other factors need to be considered to explain
370 the magnitude of the recorded SST.

371 The period of maximum SST in the Alboran Sea (11 – 9 kyr BP) occurred while the North
372 Atlantic ocean was still under the influence of meltwater pulses from the Laurentide ice
373 sheet (Fig. 5b) that injected fresh-water in to the surface north Atlantic Ocean. This
374 situation induced a stratification in the north Atlantic and consequently a weakening the
375 SPG circulation (Thornalley et al., 2009). At lower latitudes, it has been proposed that
376 the heat transport from the STG toward the north Atlantic was reduced (Repschläger et
377 al., 2017). The consequent heat accumulation in the STG could have contributed to form
378 a warmer inflow into the Mediterranean Sea and thus lead to the observed maximum
379 SST in the Alboran Sea (Fig. 5c). But it is also relevant to note that this early Holocene
380 warm period (11 – 9 kyr BP) in the Alboran Sea corresponds to the last stage of an
381 organic rich layer (ORL) formation (Fig. 5e). This ORL has been associated to a strong
382 western Mediterranean stratification phase lead by the deglacial sea level rise reducing
383 the vertical mixing. (Cacho et al., 2002; Rogerson et al., 2008). As a consequence of this
384 situation, the modification of Atlantic inflow through its path into the Mediterranean could
385 be reduced and thus favouring the persistence of the warm conditions of the inflowing
386 subtropical waters.

387 At around 9 kyr BP, the Alboran SST record (Fig. 5c) starts a progressive cooling trend
388 that culminates reaching the minimum values at around 4.2 ka BP. The onset of this



389 cooling trend is coincident with the development of a well-mixed surface layer (Fig. 5b)
390 in the North Atlantic due to the reduction of the deglacial melting (Thornalley et al., 2009).
391 This situation would have allowed an enhanced transport of subtropical waters towards
392 higher latitudes, releasing the previous heat accumulation in the STG and potentially,
393 leading to the entrance of a cooler inflow into the Mediterranean Sea. In addition, 9 kyr
394 BP also marked the end of the Western Mediterranean stratification phase that led the
395 formation of the last ORL in the Alboran Sea (Fig. 5e). This end occurred at the time of
396 a strong increase in the speed of deep water currents (Fig. 5d) associated with the
397 formation of the Western Mediterranean Deep Waters (Frigola et al., 2007). The
398 reduction in surface stratification in the Alboran Sea would have led to an increased
399 water mixing of the inflowing Atlantic waters that could contribute to the observed cooling
400 trend. This situation was apparently also linked to an increase in the local upwelling
401 conditions developed by the establishment of the western anticyclonic gyre of the
402 Alboran Sea that, according to coccolith assemblages, occurred after 7.7 kyr BP (Ausin
403 et al., 2015). In addition, the described SST cooling trend for this period, could also be
404 promoted by some additional atmospheric forcing. Several authors have suggested a
405 southward displacement of North Atlantic westerlies during this period, inducing a
406 southern penetration of winter storm tracks (Desprat et al., 2013; Fletcher et al., 2012;
407 Chabaud et al., 2014; Zielhofer et al., 2017). Therefore, a combination of factors, internal
408 and external to the Alboran Sea could have accounted for the observed SST cooling
409 trend after 9 kyr and until 4.2 kyr BP, when a change occurred in both long and short
410 term variability.

411 At about 4.2 kyr BP a double peak structure of minimum SST occurred (Fig. 5c) reaching
412 ~12.8°C and representing the minimum values of the record. After this event, the long
413 term cooling trend ceased while an intense millennial-scale variability developed,
414 involving SST oscillations over 2°C. This event is apparently synchronous with a peak
415 in the record of deep water current intensity (Fig. 5d) suggesting that deep convection



416 was strengthened in the Western Mediterranean Sea during this 4.2 event, but not more
417 than during other previous and later Holocene events of this record (Frigola et al., 2007).
418 On another hand, the North Atlantic record (Fig. 5b) indicates that the 4.2 cold SST over
419 the Alboran Sea correspond to one of the millennial scale stratification events that
420 occurred along the Holocene, interpreted as a weak mode of SPG circulation (Thornalley
421 et al., 2009). This situation contrasts with that observed during the early Holocene period,
422 when weak SPG circulation coexisted with maximum SST in the Alboran Sea.
423 Interestingly, after the 4.2 event, during the late Holocene, both the Alboran record and
424 also the North Atlantic record show an intense millennial-scale variability, with minimums
425 in Alboran SST occurring systematically during periods of weak SPG circulation (Fig 5b
426 and c). However, further information would be required to establish a mechanism that
427 could potentially link these apparent changes in late Holocene AMOC and properties in
428 the Atlantic inflow in the Alboran Sea.

429 A further insight into the Holocene evolution of the inflowing Atlantic water into the
430 Mediterranean Sea comes from the observation of the obtained ALB-2 $\delta^{18}\text{O}_{\text{sw}}$
431 reconstruction (Fig. 5f). This record also differentiates three Holocene periods consistent
432 with those defined in base to the SST record (Fig. 5c). The ALB-2 $\delta^{18}\text{O}_{\text{sw}}$ record is
433 compared with another $\delta^{18}\text{O}_{\text{sw}}$ record (Fig. 5g) that reflects conditions of the subsurface
434 waters from the subtropical gyre (Repschläger et al., 2017). Interestingly, the relation
435 between these two records change for the three defined Holocene intervals (Fig. 5f and
436 g). During the early Holocene Alboran waters were heavier than those from the STG as
437 should be expected for an inflowing modified water after mixing with Mediterranean
438 source isotopic heavier water masses. During the middle Holocene phase, while
439 Alboran-SST followed a cooling trend, the $\delta^{18}\text{O}_{\text{sw}}$ record oscillates around its lightest
440 values, even lighter than those from the STG during the same period, and this difference
441 became larger across the interval (Fig. 5f and g). Such a situation could suggest that the
442 inflowing waters into the Mediterranean Sea are also feeding by some lighter water mass



443 likely from a higher latitude source. This is consistent with the previous discussed
444 enhanced transport of subtropical waters towards higher latitudes during this period that
445 would have led, to a stronger southward influence SPG source waters that would
446 ultimately get into the Atlantic inflowing waters. This situation would be coherent with the
447 described intensification of the SPG by Thornalley et al. (2009) and the dominant
448 influence of subpolar source central waters at intermediate depths of the mid-latitude
449 North Atlantic (Colin et al., 2010). After the 4.2 event the STG and Alboran $\delta^{18}\text{O}_{\text{sw}}$ records
450 converge to similar values (Fig. 5f and g). This supports a reduced southward influence
451 of SPG waters during the late Holocene, consistent with the interpreted STG source of
452 intermediate waters in the mid-latitude North Atlantic (Colin et al., 2010) and the end of
453 the mid Holocene SST cooling trend described previously for the Alboran Sea. The late
454 Holocene millennial scale variability is difficult to characterise in this Atlantic-
455 Mediterranean $\delta^{18}\text{O}_{\text{sw}}$ comparison (Fig. 5f and g) due to uncertainties in the relative
456 chronologies and errors in the proxy reconstruction. Thus further information needs to
457 be explored to ultimately determine the nature of a potential late Holocene Atlantic-
458 Mediterranean millennial scale connection.

459

460 5. CONCLUSIONS

461 The analysis of Mg/Ca derived SST and the $\delta^{18}\text{O}$ from the ALB-2 record have allowed
462 the reconstruction of the paleoceanography of the Alboran Sea during the Holocene and
463 its possible interactions with the Atlantic Ocean. The comparison of new generated
464 oxygen isotopes ($\delta^{18}\text{O}$) and Mg/Ca-SST records from ALB-2 with the others western
465 Mediterranean records confirms a common oceanographic signal and evidences the fast
466 modification of the Atlantic Water Inflow in to a more Mediterranean signal likely reflecting
467 surface mixing with the underlying Mediterranean waters.



468 This multi-core comparison of the Western Mediterranean *G. bulloides* Mg/Ca-SST
469 signal, strongly supports the value of this proxy to reconstruct true regional
470 environmental conditions. However, when Mg/Ca-SST records are compared with the
471 previously published alkenone-SST records significant differences emerge. This proxy
472 comparison is extended to the glacial period, observing a major proxy difference during
473 the deglaciation, particularly during the second warming phase occurring after the YD
474 period, which is almost absent in all the Mg/Ca-SST records. We interpret that this
475 damped warming in the Mg/Ca record reflects a resilient capacity of *G. bulloides* to
476 change the growth season in order to compensate the large SST deglacial warming
477 (above 8°C according to the alkenone-SST record). In this regard, we argued that during
478 the last glacial period and the first part of the deglaciation, *G. bulloides* would have mostly
479 grown during the milder upwelling season (autumn) while, after the YD, *G. bulloides*
480 minimized the impact of the warming by developing mostly during the colder upwelling
481 season, (spring) which is also the current situation. In contrast, during the Holocene, the
482 SST variability is far larger in the Mg/Ca-SST record (~5°C) than in the alkenone-SST
483 record (~2°C). We interpreted this Mg/Ca-SST variability as a true climate evolution of a
484 single season, spring, while the reduced variability in the alkenone-SST responds to a
485 well averaged annual signal.

486 The new high resolution Holocene Mg/Ca-SST record differentiates three intervals
487 according to its main patterns: (1) The warmest SST values occurred during the Early
488 Holocene (11.7 – 9 kyr BP); (2) During the middle Holocene occurred a continuous
489 cooling trend that culminated with the coldest Holocene SST in a double peak structure
490 centred at around 4.2 kyr BP; (3) The Late Holocene (4.2 kyr BP to the present) did not
491 follow any clear cooling/warming trend but millennial-scale oscillations were enhanced.
492 This general Holocene SST evolution matches to some extent solar energy
493 redistribution by the changing orbital configuration, nevertheless, the intensity of the
494 changes and the short term variability requires of the action of some other factors.



495 The warmest SST of the Early Holocene (11 – 9 kyr BP) occurred while intense meltwater
496 pulses from the Laurentide ice sheet could have led to a reduction in the northward heat
497 transport from the STG towards north Atlantic, the consequent heat accumulation could
498 have contributed to the warm inflow in to the Mediterranean Sea. These warm conditions
499 could also be favoured by the enhanced surface stratification in the Western
500 Mediterranean that lead the last ORL formation.

501 The onset of the cooling trend occurred at 9 kyr BP and was coincident with the re-
502 establishment of well-mixed surface and deep water layers that ended the ORL
503 deposition in the Alboran Sea. This long term cooling trend is also coincident with the
504 increase of the upwelling conditions on the Alboran Sea and with a described southward
505 displacement of the North Atlantic westerlies. The relative evolution of the $\delta^{18}\text{O}_{\text{sw}}$ records
506 from Alboran sea and the STG suggest the arrival through Gibraltar of light waters from
507 northern latitudes, supporting a enhance influence of high latitudes north Atlantic
508 conditions in the inflowing waters to the Mediterranean Sea. In summary, the described
509 middle Holocene SST-cooling trend could reflect a complex interaction of external and
510 internal factors into this Mediterranean region.

511 The 4.2 kyr BP event is recorded in the Mg/Ca-SST as a double peak event, reaching
512 the lowest SST of the Holocene, and it ended the cooling trend of the previous interval.
513 This 4.2 event marks the onset of an intense millennial-scale variability that dominated
514 during the Late Holocene and that coincides with an event of intense WMDW formation.
515 A comparable millennial-scale variability has been previously described further north in
516 the North Atlantic Ocean, in relation to the intensity of the SPG. The ultimate connections
517 between these North Atlantic changes and Alboran Sea need of further information to be
518 fully understood but our observations highlight that the Atlantic-Mediterranean
519 connections through the inflow operated in a different way during the Early and Late
520 Holocene.

521



522 **Acknowledgments**

523 Core ALB-2 was recovered by the HERMESIONE expedition onboard R/V Hespérides
524 in 2009. This research has been financially supported by OPERA project (CTM2013-
525 48639-C2-1-R), CHIMERA project (CTM2016-75411-R) and for TIMED project
526 (683237). Leopoldo Pena acknowledges support from the Ramón y Cajal program
527 (MINECO, Spain). We thank Generalitat de Catalunya Grups de Recerca Consolidats
528 for grant 2017 SGR 315 to GRC Geociències Marines. We are grateful to M. Guart (Dept.
529 Dinàmica de la Terra i de l'Oceà, Universitat de Barcelona), M. Romero, T. Padró and J.
530 Perona (Serveis Científics i Tècnics, Universitat de Barcelona). We also acknowledge
531 the guest editor and the anonymous reviewers for their comments, which contributed to
532 improving this paper.



533 **REFERENCES**

534

535 Andrews, J. T., Hardadottir, J., Stoner, J. S., Mann, M. E., Kristjansdottir, G. B. and
536 Koc, N.: Decadal to millennial-scale periodicities in North Iceland shelf sediments over
537 the last 12 000 cal yr: long-term North Atlantic oceanographic variability and solar
538 forcing, *Earth Planet. Sci. Lett.*, 210, 453–465, doi:10.1016/S0012-821X(03)00139-0,
539 2003.

540 Ausin, B., Flores, J. A., Sierro, F. J., Cacho, I., Hernández-Almeida, I., Martrat, B. and
541 Grimalt, J. O.: Atmospheric patterns driving Holocene productivity in the Alboran Sea
542 (Western Mediterranean): A multiproxy approach, *The Holocene*, 25(4), 583–595,
543 doi:10.1177/0959683614565952, 2015.

544 Bárcena, M. A., Flores, J. A., Sierro, F. J., Pérez-Folgado, M., Fabres, J., Calafat, A.
545 and Canals, M.: Planktonic response to main oceanographic changes in the Alboran
546 Sea (Western Mediterranean) as documented in sediment traps and surface
547 sediments, *Mar. Micropaleontol.*, 53(3–4), 423–445,
548 doi:10.1016/j.marmicro.2004.09.009, 2004.

549 Barker, S., Greaves, M. and Elderfield, H.: A study of cleaning procedures used for
550 foraminiferal Mg/Ca paleothermometry, *Geochemistry, Geophys. Geosystems*, 4(9), 1–
551 20, doi:10.1029/2003GC000559, 2003.

552 Bartlein, P. J., Harrison, S. P., Brewer, S., Connor, S., Davis, B. A. S., Gajewski, K.,
553 Guiot, J., Henderson, A., Peyron, O., Prentice, I. C., Scholze, M., Seppä, H., Shuman,
554 B., Sugita, S., Thompson, R. S., Viau, A. E., Williams, J. and Wu, H.: Pollen-based
555 continental climate reconstructions at 6 and 21 ka: a global synthesis, *Clim. Dyn.*, 37,
556 775–802, doi:10.1007/s00382-010-0904-1, 2011.

557 Blaauw, M. and Christen, J. A.: Bacon manual – v2.2, , 1–11, 2011.

558 Béthoux, J. P.: Mean water fluxes across sections in the Mediter- ranean Sea,
559 evaluated in the basis of water and salt budgets and of observed salinities, *Oceanol.*
560 *Acta*, 3, 79–88, 1980.

561 Bond, G., Showers, W., Cheseby, M., Lotti, R., Almasi, P., DeMenocal, P., Priore, P.,
562 Cullen, H., Hajdas, I. and Bonani, G.: A Pervasive Millennial-Scale Cycle in North
563 Atlantic Holocene and Glacial Climates, *Science (80-)*, 278(5341), 1257–1266,
564 doi:10.1126/science.278.5341.1257, 1997.

565 Bond, G., Kromer, B., Beer, J., Muscheler, R., Evans, M. N., Showers, W., Hoffmann,
566 S., Lotti-Bond, R., Hajdas, I. and Bonani, G.: Persistent Solar Influence on North
567 Atlantic Climate During the Holocene, *Science (80-)*, 294(2001), 2130–2136,
568 doi:10.1126/science.1065680, 2001.

569 Böning, C. W., Scheinert, M., Dengg, J., Biastoch, A. and Funk, A.: Decadal variability
570 of subpolar gyre transport and its reverberation in the North Atlantic overturning,
571 *Geophys. Res. Lett.*, 33, 1–5, doi:10.1029/2006GL026906, 2006.

572 Bray, N. A., Ochoa, J. and Kinder, T. H.: The role of the interface exchange through the
573 Strait of Gibraltar, *J. Geophys. Res.*, 100(C6), 10755–176, doi:10.1029/95JC00381,
574 1995.

575 Cacho, I., Grimalt, J. O., Pelejero, C., Canals, M., Sierro, F. J., Flores, J. A. and
576 Shackleton, N.: Dansgaard-Oeschger and Heinrich event imprints in Alboran Sea
577 paleotemperatures, *Paleoceanography*, 14(6), 698–705,
578 doi:<https://doi.org/10.1029/1999PA900044>, 1999.



- 579 Cacho, I., Grimalt, J. O., Canals, M., Sbaffi, L., Shackleton, N. J., Schönfeld, J. and
580 Zahn, R.: Variability of the western Mediterranean Sea surface temperature during the
581 last 25,000 years and its connection with the Northern Hemisphere climatic changes,
582 *Paleoceanography*, 16(1), 40–52, doi:10.1029/2000PA000502, 2001.
- 583 Cacho, I., Grimalt, J. O. and Canals, M.: Response of the Western Mediterranean Sea
584 to rapid climatic variability during the last 50,000 years: A molecular biomarker
585 approach, *J. Mar. Syst.*, 33–34, 253–272, doi:10.1016/S0924-7963(02)00061-1, 2002.
- 586 Chabaud, L., Sánchez Goñi, M. F., Desprat, S. and Rossignol, L.: Land–sea climatic
587 variability in the eastern North Atlantic subtropical region over the last 14,200 years:
588 Atmospheric and oceanic processes at different timescales, *The Holocene*, 24(7), 787–
589 797, doi:10.1177/0959683614530439, 2014.
- 590 Cisneros, M., Cacho, I., Frigola, J., Canals, M., Masqué, P., Martrat, B., Casado, M.,
591 Grimalt, J. O., Pena, L. D., Margaritelli, G. and Lirer, F.: Sea surface temperature
592 variability in the central-western Mediterranean Sea during the last 2700 years: A multi-
593 proxy and multi-record approach, *Clim. Past*, 12(4), 849–869, doi:10.5194/cp-12-849-
594 2016, 2016.
- 595 Cléroux, C., Debret, M., Cortijo, E., Duplessy, J.-C., Dewilde, F., Reijmer, J. and
596 Massei, N.: High-resolution sea surface reconstructions off Cape Hatteras over the last
597 10 ka, *Paleoceanography*, 27(1), 1–14, doi:10.1029/2011PA002184, 2012.
- 598 Colin, C., Frank, N., Copard, K. and Douville, E.: Neodymium isotopic composition of
599 deep-sea corals from the NE Atlantic: implications for past hydrological changes during
600 the Holocene, *Quat. Sci. Rev.*, 29(19–20), 2509–2517,
601 doi:10.1016/j.quascirev.2010.05.012, 2010.
- 602 Combourieu Nebout, N., Turon, J., Zahn, R., Capotondi, L., Lon- deix, L., and Pahnke,
603 K.: Enhanced aridity and atmospheric high-pressure stability over the western
604 Mediterranean during the North Atlantic cold events of the past 50 k.y., *Geology*, 30,
605 863– 866, 2002.
- 606 Combourieu Nebout, N., Peyron, O., Dormoy, I., Desprat, S., Beaudouin, C., Kotthoff,
607 U. and Marret, F.: Rapid climatic variability in the west Mediterranean during the last 25
608 000 years from high resolution pollen data, *Clim. Past*, 5, 503–521,
609 doi:<https://doi.org/10.5194/cp-5-503-2009>, 2009.
- 610 Coplen, T. B.: New guidelines for reporting stable hydrogen, carbon, and oxygen
611 isotope-ratio data, *Geochim. Cosmochim. Acta*, 60(17), 3359–3360,
612 doi:[https://doi.org/10.1016/0016-7037\(96\)00263-3](https://doi.org/10.1016/0016-7037(96)00263-3), 1996.
- 613 Debret, M., Bout-Roumazeilles, V., Grousset, F., Desmet, M., Mcmanus, J. F., Massei,
614 N., Sebag, D., Petit, J.-R., Copard, Y. and Trentesaux, A.: The origin of the 1500-year
615 climate cycles in Holocene North-Atlantic records, *Clim. Past*, 3, 569–575,
616 doi:<https://doi.org/10.5194/cp-3-569-2007>, 2007.
- 617 Debret, M., Sebag, D., Crosta, X., Massei, N., Petit, J.-R., Chapron, E. and Bout-
618 Roumazeilles, V.: Evidence from wavelet analysis for a mid-Holocene transition in
619 global climate forcing, *Quat. Sci. Rev.*, 28(25–26), 2675–2688,
620 doi:10.1016/j.quascirev.2009.06.005, 2009.
- 621 Desprat, S., Combourieu-Nebout, N., Essallami, L., Sicre, M. A., Dormoy, I., Peyron,
622 O., Siani, G., Bout Roumazeilles, V. and Turon, J. L.: Deglacial and holocene
623 vegetation and climatic changes in the southern central Mediterranean from a direct
624 land-sea correlation, *Clim. Past*, 9(2), 767–787, doi:10.5194/cp-9-767-2013, 2013.



- 625 Elderfield, H. and Ganssen, G.: Past temperature and delta18O of surface ocean
626 waters inferred from foraminiferal Mg/Ca ratios, *Nature*, 405(6785), 442–445,
627 doi:10.1038/35013033, 2000.
- 628 Fletcher, W. J., Debret, M. and Sanchez-Goñi, M.-F.: Mid-Holocene emergence of a
629 low-frequency millennial oscillation in western Mediterranean climate: Implications for
630 past dynamics of the North Atlantic atmospheric westerlies, *The Holocene*, 0, 1–14,
631 doi:10.1177/0959683612460783, 2012.
- 632 Frigola, J., Moreno, A., Cacho, I., Canals, M., Sierro, F. J., Flores, J. A., Grimalt, J. O.,
633 Hodell, D. A. and Curtis, J. H.: Holocene climate variability in the western
634 Mediterranean region from a deepwater sediment record, *Paleoceanography*, 22, 2209,
635 doi:10.1029/2006PA001307, 2007.
- 636 Frigola, J., Moreno, A., Cacho, I., Canals, M., Sierro, F. J., Flores, J. A. and Grimalt, J.
637 O.: Evidence of abrupt changes in Western Mediterranean Deep Water circulation
638 during the last 50 kyr: A high-resolution marine record from the Balearic Sea, *Quat. Int.*,
639 181(1), 88–104, doi:10.1016/j.quaint.2007.06.016, 2008.
- 640 Fiúza, A.F.G.: Hidrologia e dinamica das aguas costeiras de Portugal. Ph.D. Thesis,
641 Universidade de Lisboa, 1984
- 642 Gao, Y.-Q. and Yu, L.: Subpolar Gyre Index and the North Atlantic Meridional
643 Overturning Circulation in a Coupled Climate Model, *Atmos. Ocean. Sci. Lett.*, 1(1),
644 29–32, 2008.
- 645 Giraudeau, J., Grelaud, M., Solignac, S., Andrews, J. T., Moros, M. and Jansen, E.:
646 Millennial-scale variability in Atlantic water advection to the Nordic Seas derived from
647 Holocene coccolith concentration records, *Quat. Sci. Rev.*, 29(9–10), 1276–1287,
648 doi:10.1016/j.quascirev.2010.02.014, 2010.
- 649 Hemleben, C., Spindler, Anderson, M., O. Roger. *Modern Planktonic Foraminifera*.
650 Springer, Berlin, 1989
- 651 Hernández-Almeida, I., Bárcena, M. A., Flores, J. A., Sierro, F. J., Sanchez-Vidal, A.
652 and Calafat, A.: Microplankton response to environmental conditions in the Alboran
653 Sea (Western Mediterranean): One year sediment trap record, *Mar. Micropaleontol.*,
654 78(1–2), 14–24, doi:10.1016/j.marmicro.2010.09.005, 2011.
- 655 Jalali, B., Sicre, M.-A., Bassetti, M.-A. and Kallel, N.: Holocene climate variability in the
656 North-Western Mediterranean Sea (Gulf of Lions), *Clim. Past*, 12, 91–101,
657 doi:10.5194/cp-12-91-2016, 2016.
- 658 Jiménez-Amat, P. and Zahn, R.: Offset timing of climate oscillations during the last two
659 glacial-interglacial transitions connected with large-scale freshwater perturbation,
660 *Paleoceanography*, 30, 768–788, doi:10.1002/2014PA002710, 2015.
- 661 Kemle-von Mücke, S., and Hemleben, C.: Foraminifera. In: Boltovskoy, D. (Ed.), *South*
662 *Atlantic Zooplankton*. Backhuys Publishers, Leiden, The Netherlands, 1999
- 663 Kim, J.-H., Rimbu, N., Lorenz, S. J., Lohmann, G., Nam, S., Schouten, S., Ru, C. and
664 Schneider, R. R.: North Pacific and North Atlantic sea-surface temperature variability
665 during the Holocene, *Quat. Sci. Rev.*, 23, 2141–2154,
666 doi:10.1016/j.quascirev.2004.08.010, 2004.
- 667 Kucera, M. and Darling, K. F.: Cryptic species of planktonic foraminifera: their effect on
668 palaeoceanographic reconstructions, *R. Soc.*, 360, 695–718,
669 doi:10.1098/rsta.2001.0962, 2002.



- 670 Kucera, M., Weinelt, M., Kiefer, T., Pflaumann, U., Hayes, A., Weinelt, M., Chen, M.
671 Te, Mix, A. C., Barrows, T. T., Cortijo, E., Duprat, J., Juggins, S. and Waelbroeck, C.:
672 Reconstruction of sea-surface temperatures from assemblages of planktonic
673 foraminifera: multi-technique approach based on geographically constrained calibration
674 data sets and its application to glacial Atlantic and Pacific Oceans, *Quat. Sci. Rev.*,
675 24(7–9 SPEC. ISS.), 951–998, doi:10.1016/j.quascirev.2004.07.014, 2005.
- 676 Lacombe, H., Gascard, J. C., Cornella, J., and Béthoux, J. P.: Re- sponse of the
677 Mediterranean to the water and energy fluxes across its surface, on seasonal and
678 interannual scales, *Oceanol. Acta*, 4, 247–255, 1981.
- 679 Laepple, T., and P. Huybers: Reconciling discrepancies between Uk37 and Mg/Ca
680 reconstructions of Holocene marine temperature variability, *Earth Planet. Sci. Lett.*,
681 375, 418–429, 2013.
- 682 Lionello, P., Malanotte-Rizzoli, P., Boscolo, R., Alpert, P., Artale, V., Li, L., Luterbacher,
683 J., May, W., Trigo, R., Tsimplis, M., Ulbrich, U. and Xoplaki, E.: The Mediterranean
684 climate: An overview of the main characteristics and issues, *Dev. Earth Environ. Sci.*,
685 4(C), 1–26, doi:10.1016/S1571-9197(06)80003-0, 2006.
- 686 Lorenz, S. J. and Lohmann, G.: Acceleration technique for Milankovitch type forcing in
687 a coupled atmosphere-ocean circulation model : method and application for the
688 Holocene, *Clim. Dyn.*, 23, 727–743, doi:10.1007/s00382-004-0469-y, 2004.
- 689 Marchal, O., Cacho, I., Stockera, T. F., Grimalt, J. O., Calvo, E., Martrat, B.,
690 Shackleton, N., Vautravers, M., Cortijo, E., Kreveld, S. van, Andersson, C., Koç, N.,
691 Chapman, M., Saffi, L., Duplessy, J.-C., Sarnthein, M., Turon, J.-L., Duprat, J. and
692 Jansen, E.: Apparent long-term cooling of the sea surface in the northeast Atlantic and
693 Mediterranean during the Holocene, *Quat. Sci. Rev.*, 21, 455–483, doi:10.1016/S0277-
694 3791(01)00105-6, 2002.
- 695 Marchitto, T. M. and DeMenocal, P. B.: Late Holocene variability of upper North Atlantic
696 Deep Water temperature and salinity, *Geochemistry, Geophys. Geosystems*, 4(12),
697 1100, doi:10.1029/2003GC000598, 2003.
- 698 Martrat, B., Grimalt, J. O., Lopez-Martínez, C., Cacho, I., Sierro, F. J., Flores, J. A.,
699 Zhang, R., Canals, M., Curtis, J. H. and Hodell, D. A.: Abrupt Temperature changes in
700 the Western Mediterranean over the past 250,000 years, *Science* (80-), 306(5702),
701 1762–1765, doi:10.1126/science.1101706, 2004.
- 702 Martrat, B., Jimenez-amat, P., Zahn, R. and Grimalt, J. O.: Similarities and
703 dissimilarities between the last two deglaciations and interglaciations in the North
704 Atlantic region, *Quat. Sci. Rev.*, 99, 122–134, doi:10.1016/j.quascirev.2014.06.016,
705 2014.
- 706 McCartney, M. S. and Talley, L. D.: The subpolar mode water of North Atlantic Ocean,
707 *Am. Meteorol. Soc.*, 12, 1169–1188, doi:[https://doi.org/10.1175/1520-0485\(1982\)012<1169:TSMWOT>2.0.CO;2](https://doi.org/10.1175/1520-0485(1982)012<1169:TSMWOT>2.0.CO;2), 1982.
- 709 Millot, C.: Circulation in the Western Mediterranean Sea, *J. Mar. Syst.*, 20, 423–442,
710 doi:10.1016/S0924-7963(98)00078-5, 1999.
- 711 Millot, C.: Progress in Oceanography Another description of the Mediterranean Sea
712 outflow, *Prog. Oceanogr.*, 82(2), 101–124, doi:10.1016/j.pocean.2009.04.016, 2009.
- 713 Moreno, A., Cacho, I., Canals, M., Prins, M. A., Sánchez-Goñi, M.-F., Grimalt, J. O.
714 and Weltje, G. J.: Saharan Dust Transport and High-Latitude Glacial Climatic
715 Variability: The Alboran Sea Record, *Quat. Res.*, 58, 318–328,
716 doi:10.1006/qres.2002.2383, 2002.



- 717 Moros, M., Emeis, K., Risebrobakken, B., Snowball, I., Kuijpers, A., McManus, J. and
718 Jansen, E.: Sea surface temperatures and ice rafting in the Holocene North Atlantic:
719 climate influences on northern Europe and Greenland, *Quat. Sci. Rev.*, 23(20–22
720 SPEC. ISS.), 2113–2126, doi:10.1016/j.quascirev.2004.08.003, 2004.
- 721 Nieto-Moreno, V., Martínez-Ruiz, F., Giral, S., Gallego-Torres, D., García-Orellana, J.,
722 Masqué, P. and Ortega-Huertas, M.: Climate imprints during the “Medieval Climate
723 Anomaly” and the “Little Ice Age” in marine records from the Alboran Sea basin, *The
724 Holocene*, 0(0), 1–11, doi:10.1177/0959683613484613, 2013.
- 725 Pena, L. D., Calvo, E., Cacho, I., Eggins, S. and Pelejero, C.: Identification and
726 removal of Mn-Mg-rich contaminant phases on foraminiferal tests: Implications for
727 Mg/Ca past temperature reconstructions, *Geochemistry, Geophys. Geosystems*, 6(9),
728 doi:10.1029/2005GC000930, 2005.
- 729 Prah, F., Herbert, T., Brassell, S. C., Ohkouchi, N., Pagani, M., Repeta, D., Rosell-
730 Melé, A. and Sikes, E.: Status of alkenone paleothermometer calibration: Report from
731 Working Group 3, *Geochemistry, Geophys. Geosystems*, 1(11),
732 doi:10.1029/2000GC000058, 2000.
- 733 Rao, K. K., Paulinose, V. T., Jayalakshmy, K. V., Panikkar, B. M. and Krishnan Kutty,
734 M.: Distribution of Living Planktonic Foraminifera in the Coastal Upwelling Region of
735 Kenya, Africa, *Indian J. Mar. Sediments*, 17(2), 121–127, 1988.
- 736 Reimer, P. J., Bard, E., Bayliss, A., Beck, J. W., Blackwell, P. G., Bronk, C., Caitlin, R.,
737 Hai, E. B., Edwards, R Lawrence Friedrich, M., Grootes, P. M., Guilderson, T. P.,
738 Hafliadason, H., Hajdas, I., Hatté, C., Heaton, T. J., Hoffmann, D. L., Hogg, A. G.,
739 Hughen, K. A., Kaiser, K. F., Kromer, B., Manning, S. W., Niu, M., Reimer, R. W.,
740 Richards, D. A., Scott, E. M., Southon, J. R., Staff, R. A., Turney, C. S. M. and van der
741 Plicht, J.: INTCAL13 AND MARINE13 RADIOCARBON AGE CALIBRATION CURVES
742 0–50,000 YEARS CAL BP, *Radiocarbon*, 55(4), 1869–1887,
743 doi:https://doi.org/10.2458/azu_js_rc.55.16947, 2013.
- 744 Repschläger, J., Garbe-Schönberg, D., Weinelt, M. and Schneider, R.: Holocene
745 evolution of the North Atlantic subsurface transport, *Clim. Past Discuss.*, 13, 333–344,
746 doi:10.5194/cp-2016-115, 2017.
- 747 Rigual-Hernández, A. S., Sierro, F. J., Bárcena, M. A., Flores, J. A., and Heussner, S.:
748 Seasonal and interannual changes of planktic foraminiferal fluxes in the Gulf of Lions
749 (NW Mediterranean) and their implications for paleoceanographic studies: two 12- year
750 sediment trap records, *Deep-Sea Res. Pt. I*, 66, 26–40, doi:10.1016/j.dsr.2012.03.011,
751 2012. Rigual-Hernández,
- 752 Rimbu, N., Lohmann, G., Lorenz, S. J., Kim, J. H. and Schneider, R. R.: Holocene
753 climate variability as derived from alkenone sea surface temperature and coupled
754 ocean-atmosphere model experiments, *Clim. Dyn.*, 23, 215–227, doi:10.1007/s00382-
755 004-0435-8, 2004.
- 756 Roberts, N., Moreno, A., Valero-Garcés, B. L., Corella, J. P., Jones, M., Allcock, S.,
757 Woodbridge, J., Morellón, M., Luterbacher, J., Xoplaki, E. and Türkeş, M.:
758 Palaeolimnological evidence for an east–west climate see-saw in the Mediterranean
759 since AD 900, *Glob. Planet. Change*, 84–85, 23–34,
760 doi:10.1016/j.gloplacha.2011.11.002, 2012.
- 761 Rodrigo-Gámiz, M., Martínez-Ruiz, F., Jiménez-Espejo, F. J., Gallego-Torres, D.,
762 Nieto-Moreno, V., Romero, O. and Ariztegui, D.: Impact of climate variability in the
763 western Mediterranean during the last 20,000 years: oceanic and atmospheric



- 764 responses, *Quat. Sci. Rev.*, 30(15–16), 2018–2034,
765 doi:10.1016/j.quascirev.2011.05.011, 2011.
- 766 Rodrigo-Gámiz, M., Martínez-Ruiz, F., Rampen, S. W., Schouten, S. and Sinninghe
767 Damsté, J. S.: Sea surface temperature variations in the western Mediterranean Sea
768 over the last 20 kyr: A dual-organic proxy (UK'37 and LDI) approach,
769 *Paleoceanography*, 29, 87–98, doi:10.1002/2013PA002466.Received, 2014.
- 770 Rogerson, M., Cacho, I., Jimenez-Espejo, J., Reguera, M. I., Sierro, F. J., Martínez-
771 Ruiz, F., Frigola, J. and Canals, M.: A dynamic explanation for the origin of the western
772 Mediterranean organic-rich layers, *Geochemistry, Geophys. Geosystems*, 9(7),
773 doi:10.1029/2007GC001936, 2008.
- 774 Sabatier, P., Dezileau, L., Colin, C., Briquieu, L., Bouchette, F., Martinez, P., Siani, G.,
775 Raynal, O. and Von Grafenstein, U.: 7000 years of paleostorm activity in the NW
776 Mediterranean Sea in response to Holocene climate events, *Quat. Res.*, 77(1), 1–11,
777 doi:10.1016/j.yqres.2011.09.002, 2012.
- 778 Shaltout, M. and Omstedt, A.: Recent sea surface temperature trends and future
779 scenarios for the Mediterranean Sea, *Oceanologia*, 56(3), 411–443, doi:10.5697/oc.56-
780 3.411, 2014.
- 781 Sicre, M.-A., Ternois, Y., Miquel, J.-C. and Marty, J.-C.: Alkenones in the Northwestern
782 Mediterranean sea: interannual variability and vertical transfer, *Geophysical Res. Lett.*,
783 26(12), 1735–1738, doi:https://doi.org/10.1029/1999GL900353, 1999.
- 784 Sierro, F. J., Hodell, D. A., Curtis, J. H., Flores, J. A., Reguera, I., Colmenero-Hidalgo,
785 E., Bárcena, M. A., Grimalt, J. O., Cacho, I., Frigola, J. and Canals, M.: Impact of
786 icebergs melting on Mediterranean thermohaline circulation during Heinrich events,
787 *Paleoceanography*, 20(2), 1–13, doi:10.1029/2004PA001051, 2005.
- 788 Ternois, Y., Sicre, M.-A., Boireau, A., Contes, M. H. and Eglinton, G.: Evaluation of
789 long-chain alkenones as paleo-temperature indicators in the Mediterranean Sea, *Deep.
790 Res. I*, 44(2), 271–286, doi:https://doi.org/10.1016/S0967-0637(97)89915-3, 1997.
- 791 Thornalley, D. J. R., Elderfield, H. and McCave, I. N.: Holocene oscillations in
792 temperature and salinity of the surface subpolar North Atlantic, *Nature*, 457(7230),
793 711–714, doi:10.1038/nature07717, 2009.
- 794 Tinner, W., van Leeuwen, J. F. N., Colombaroli, D., Vescovi, E., van der Knaap, W. O.,
795 Henne, P. D., Pasta, S., D'Angelo, S. and La Mantia, T.: Holocene environmental and
796 climatic changes at Gorgo Basso, a coastal lake in southern Sicily, Italy, *Quat. Sci.
797 Rev.*, 28(15–16), 1498–1510, doi:10.1016/j.quascirev.2009.02.001, 2009.
- 798 Tintore, J., La Violette, P. E., Blade, I. and Cruzado, A.: A study of an intense density
799 front in eastern Alboran Sea: the Almeria-Oran Front, *J. Phys. Oceanogr.*, 18, 1384–
800 1397, doi:https://doi.org/10.1175/1520-0485(1988)018<1384:ASOAIID>2.0.CO;2, 1988.
- 801 Toucanne, S., Jouet, G., Ducassou, E., Bassetti, M., Dennielou, B., Morelle, C., Minto,
802 A., Lahmi, M., Touyet, N., Charlier, K., Lericolais, G. and Mulder, T.: A 130,000-year
803 record of Levantine Intermediate Water flow variability in the Corsica Trough, western
804 Mediterranean Sea, *Quat. Sci. Rev.*, 33, 55–73, doi:10.1016/j.quascirev.2011.11.020,
805 2012.
- 806 Trigo, R. M., Osborn, T. J. and Corte-Real, J. M.: The North Atlantic Oscillation
807 influence on Europe: climate impacts and associated physical mechanisms, *Clim. Res.*,
808 20, 9–17, doi:10.3354/cr020009, 2002.



- 809 Tzedakis, P. C.: Seven ambiguities in the Mediterranean palaeoenvironmental
810 narrative, *Quat. Sci. Rev.*, 26(17–18), 2042–2066,
811 doi:10.1016/j.quascirev.2007.03.014, 2007.
- 812 Versteegh, G. J. M., de Leeuw, J. W., Taricco, C. and Romero, A.: Temperature and
813 productivity influences on U37 K0 and their possible relation to solar forcing of the
814 Mediterranean winter, *Geochemistry, Geophys. Geosystems*, 8(9), 1–14,
815 doi:10.1029/2006GC001543, 2007.
- 816 Wanner, H., Beer, J., Bütikofer, J., Crowley, T. J., Cubasch, U., Flückiger, J., Goosse,
817 H., Grosjean, M., Joos, F., Kaplan, J. O., Küttel, M., Müller, S. A., Prentice, I. C.,
818 Solomina, O., Stocker, T. F., Tarasov, P., Wagner, M. and Widmann, M.: Mid- to Late
819 Holocene climate change : an overview, *Quat. Sci. Rev.*, 27, 1791–1828,
820 doi:10.1016/j.quascirev.2008.06.013, 2008.
- 821 Zielhofer, C., Fletcher, W. J., Mischke, S., De Batist, M., Campbell, J. F. E., Joannin,
822 S., Tjallingii, R., El Hamouti, N., Junginger, A., Stele, A., Bussmann, J., Schneider, B.,
823 Lauer, T., Spitzer, K., Strupler, M., Brachert, T. and Mikdad, A.: Atlantic forcing
824 of Western Mediterranean winter rain minima during the last 12,000 years Christoph,
825 *Quat. Sci. Rev.*, 157, 29–51, doi:10.1016/j.quascirev.2016.11.037, 2017.
- 826

827 **Figure Capture**

828

829 **Figure 1:** Schematic modern surface and central hydrography of the North Atlantic
830 currents. Basic map obtained by © 2008-2018, Marine Geoscience Data System - All
831 Rights Reserved. Warm surface currents are shown by red dashed arrows. Central
832 currents are shown by light-blue dashed arrows. Oceanographic gyres are represented
833 by blue/red soft colored circles. Abbreviations are: NAC, North Atlantic Current; AC,
834 Azores Current; PC, Portugal Current; ENACWsp, East North Atlantic Central Water
835 Subpolar; ENACWst, East North Atlantic Central Water Subtropical; SPG, Subpolar
836 Gyre; STG, Subtropical Gyre; WMDW, Western Mediterranean Deep Water; AI, Atlantic
837 Inflow; MAW, Modified Atlantic Water. Red dots black circled indicates the cores
838 locations.

839

840 **Figure 2:** Comparison of $\delta^{18}\text{O}$ (VPDB) records and their ^{14}C calibrated dates from the
841 western Mediterranean sea along the last 17 cal. kyr BP. (a) $\delta^{18}\text{O}$ ‰ NGRIP record. (b)
842 From the top to the base in green color ranges $\delta^{18}\text{O}$ ‰ (VPDB) records from the cores
843 ALB2, ODP976 (Combourieu-Nebot et al., 2002), MD95-2043 (Cacho et al., 1999) and
844 MD99-22343 (Minorca Drift). Note ALB2 $\delta^{18}\text{O}$ ‰ (VPDB) record is plotted with an
845 independent y axis from the others in order to help on the figures compression. (c) ^{14}C
846 calibrated dates with the available errors from each record shown above. Each date is
847 colored with the same color as the record excluding the yellow dots which represents the
848 tie-points.

849

850 **Figure 3:** Western Mediterranean SST multi-record comparison for the last 17 cal. kyr
851 BP. (a) In red, summer insolation at 40°N. (b) Mg/Ca – SST (°C) from the ALB2. Light-
852 blue dots correspond to each SST result and in dark bold blue the 3 points average. Dark
853 blue arrows above the record correspond to the three Holocene intervals described in
854 the text. (c, d and e) Mg/Ca – SST (°C) from ODP976 (Jiménez-Amat and Zahn 2015),
855 MD95-2043, and MD99-2343 respectively (blue bold colored) compared with ALB-2 3
856 points average Mg/Ca – SST (°C) (black line underneath). Note that both records from
857 each plot are plotted in the same y axis. (f) Alkenones - SST (°C) from MD95-2043
858 (Cacho et al., 1999).

859

860 **Figure 4:** Western Mediterranean SST from alkenones and *G. bulloides* Mg/Ca multi-
861 comparison for the last interglacial and the following present interglacial period. Note that
862 the each following comparison have the same y axis. (a) In blue lines (ALB-2; this study
863 and ODP976; Jiménez-Amat and Zahn 2015) *G. bulloides* Mg/Ca – SST compared with
864 alkenones SST (Martrat et al., 2014) from the same ODP976 record. (b) In blue lines
865 (ALB-2 and MD95-2043; both in this study) *G. bulloides* Mg/Ca – SST compared with
866 alkenones SST from the same MD95-2043 record (Cacho et al., 1999). (c) In blue lines
867 (ALB-2 and MD99-2343; both in this study) *G. bulloides* Mg/Ca – SST compared with
868 alkenones SST from the MD95-2043 record (Cacho et al., 1999).

869

870 **Figure 5:** Holocene evolution in the Alboran Sea surface hydrography related with
871 oceanographic processes in the North Atlantic Ocean. (a) In red, the summer insolation
872 at 40°N. (b) In purple, 3 points average of density differences (kg/m^3) between *G.*
873 *bulloides* and *G. inflata* from the North Atlantic record RAPiD-12-1K (Thornalley et al.,
874 2009). (c) The new Mg/Ca – SST (°C) presented in this work from the ALB2 (Alboran



875 Sea). Light-blue dots correspond to each SST result and in dark bold blue the 3 points
876 average. (d) In brown, the UP10 fraction (%) from the Minorca drift core MD99-2343
877 (Frigola et al., 2007). (e) In grey filled line, the concentration of C_{37} alkenones in the
878 Alboran Sea record MD95-2043 (Cacho et al., 2002). (f) In green, the new $\delta^{18}O$ ‰
879 (SMOW) presented in this work from the ALB2 (Alboran Sea). (g) In orange, the
880 calculated $\delta^{18}O$ ‰ (SMOW) from the south Azores record GEOFAR-KF16 (Repschläger
881 et al 2017). Vertical bar centered: 8.4 – 9 cal kyr BP correspond to the Alboran Sea and
882 North Atlantic synchrony in oceanographic changes; 4.2 cal. kyr BP correspond to the
883 double peach structure observed in ALB-2 Mg/Ca – SST. The four vertical grey bars
884 during the Late Holocene correspond to cold events of ALB-2 Mg/Ca – SST.



Figure 1

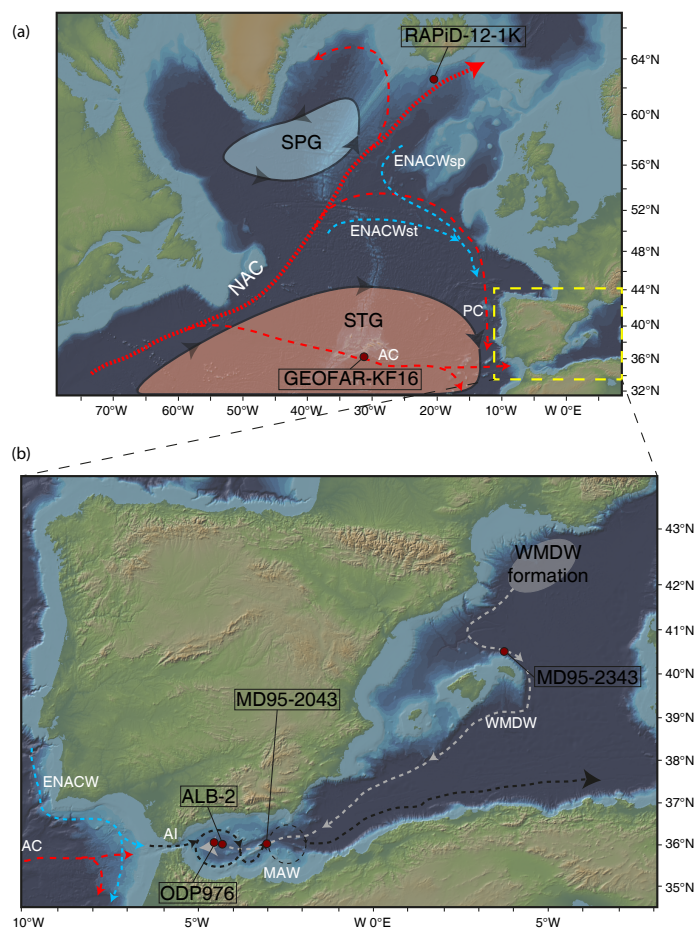




Figure 2

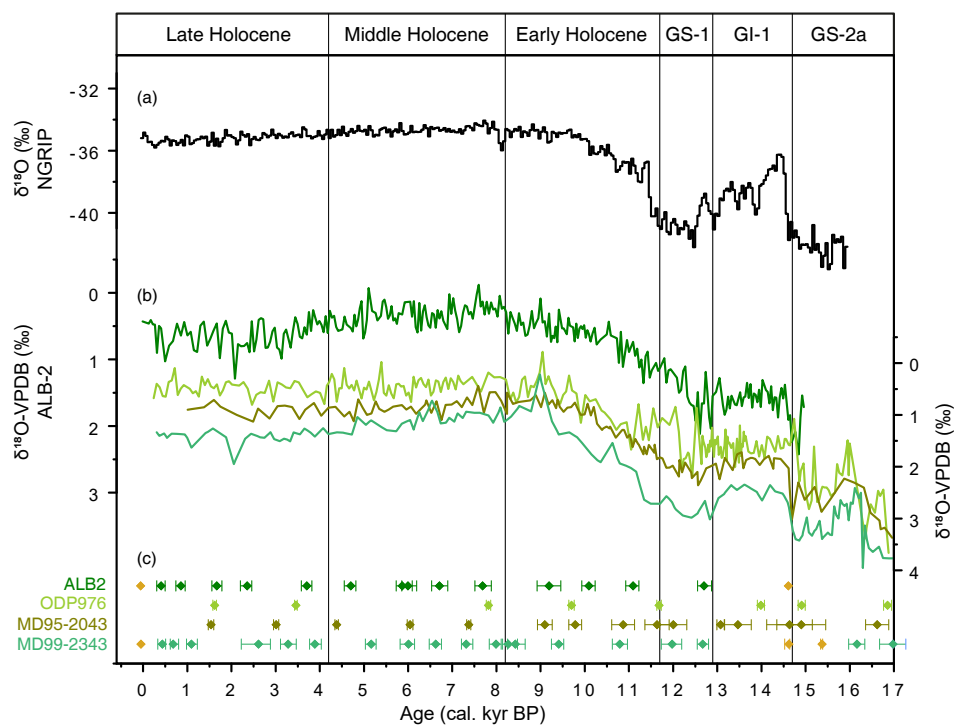




Figure 3

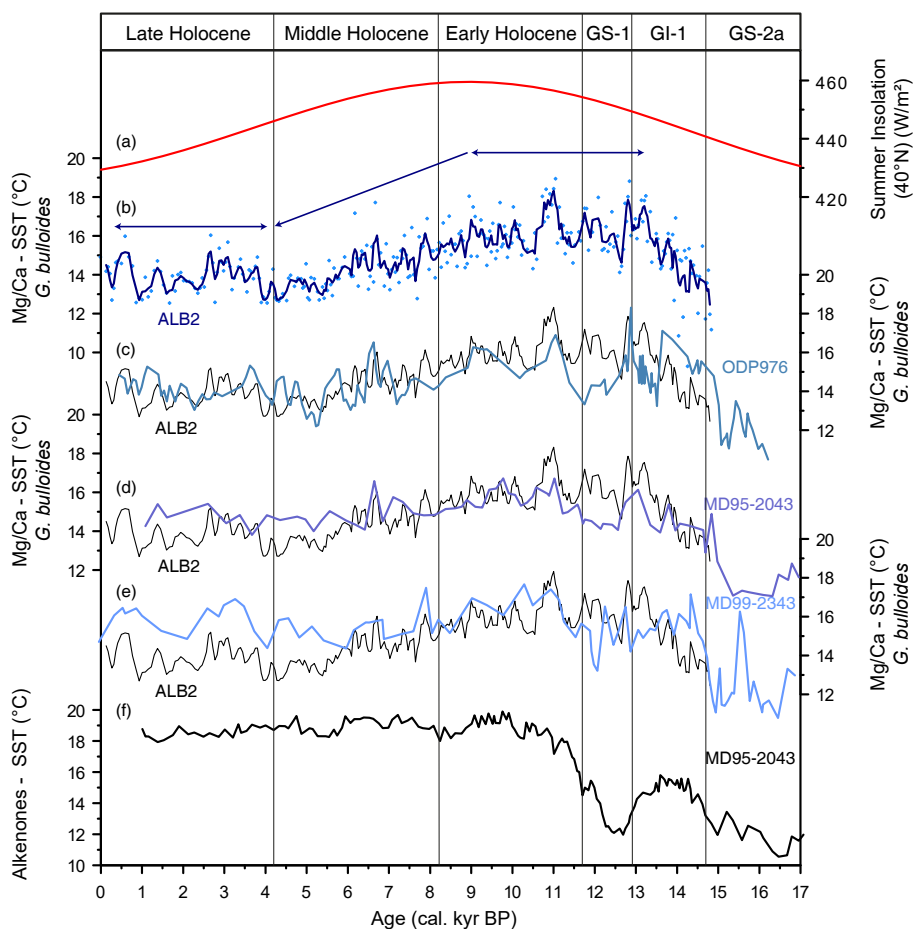




Figure 4

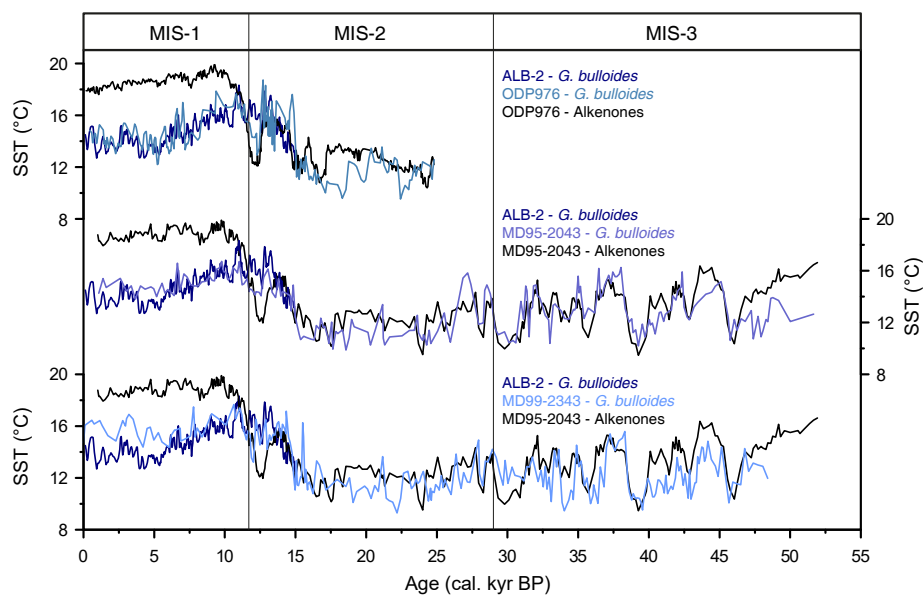




Figure 5

